ITC 1/48
Journal of Information Technology and Control
Vol. 48 / No. 1 / 2019
pp. 58-70
DOI 10.5755/j01.itc.48.1.21706

The Phase and Shift-Invariant Feature by Adaptive Independent Subspace Analysis for Cortical Complex Cells

Received 2018/09/25 | Accepted after revision 2018/12/18

crossref http://dx.doi.org/10.5755/j01.itc.48.1.21706

The Phase and Shift-Invariant Feature by Adaptive Independent Subspace Analysis for Cortical Complex Cells

Qiao Ke, Jiangshe Zhang
School of Mathematics and Statistics, Xi'an Jiaotong University, Xi'an, China 710049;
e-mail: keqiao1989@stu.xjtu.edu.cn, jszhang@mail.xjtu.edu.cn

Marcin Wozniak
Institute of Mathematics, Silesian University of Technology, Kaszubska 23, 44-100 Gliwice, Poland;
e-mail: Marcin.Wozniak@polsl.pl

Wei Wei
School of Computer Science and Engineering, Xi'an University of Technology, Xi'an 710048, China;
e-mail: weiwei@xaut.edu.cn

Corresponding author: jszhang@mail.xjtu.edu.cn

Previous studies have shown that complex cells in primary visual cortex (V1) respond selectively to the bars and edges in a specific location and orientation emerged from the natural image rather than random stimuli. In this paper, we proposed an adaptive independent subspace analysis (AISA) algorithm based on the maximum likelihood estimation of super-gaussian distribution of the norm of the partially independent components involving difference to efficiently study the characteristics of complex cells. The multiple parameters are updated with different restrictions by contrast divergence (CD) method based on the super-gaussian (sparse) distribution. In terms of the AISA results from the natural image, the inside and outside subspace of energy correlation illustrate the properties of independence. Furthermore, AISA features, similar to the response characteristics of complex cells in V1, have phase and shift-invariant, as well as frequency and orientation selectivity via the energy function of receptive fields (RFs) emerged from the tuning curve test via the sinusoidal function. Compared with the principal component analysis (PCA) filters and other ICA filters, AISA filters are analogous to Gabor filters for edge detection and human visual system via varying the frequency and orientation representation.

KEYWORDS: Independent component, phase and shift-invariant features, sparsity, gabor-like filters.

1. Introduction and Motivation

Recent advances in artificial intelligence methods have revolutionized that we process information through V1 cells by simulating how we effectively observe the physical world through the visual system to reveal the human brain's potential [16, 27, 32]. Human visual system is a computational modeling for exploring the structures of the information processing in brain based on the natural image rather than random stimulus [23, 39].

The dependent is one of the basic statistics properties generally exiting in natural image [19]. However, the features are abstractly extracted by the cells from lower layers to advance layers with a combination of linear and nonlinear transformations in human visual system [25]. The recent advances indicate the fractional areas via the response characteristics of mammal V1 neurons via the electrochemical stimulation from the visual inputs in brain [1, 33]. For instance, analyses and applications on natural image have already identified the advantages of simple cells in V1 with linear model that have adjacent elongated regions of excitation and inhibition [28].

The exploration of complex cells accelerates the further implementation of artificial intelligence (AI). Observed in the anesthetized adult cat, a small number of subunits are used to describe each RF of complex cells with a nonlinear technique, the correlation of the spike-triggered ensemble [39]. Meanwhile, complex cells are also studied by spike-triggered covariance, where the stimulus sequence are applied to identify features with trigger spikes in neurons of the anesthetized monkey with RFs containing multiple linear subunits that combine nonlinearly [15]. With the stimulus records of mammals, the complex cells respond selectively to bars and edges at a particular location and orientation kin to simple cells in V1 [35]. However, they are constant relative to the spatial phase of the stimulus [7, 36].

Independent component analysis (ICA) [3, 30] is stemmed from the blind source separation (BSS), and motivated by the human beings autonomously selecting the interesting information and ignoring the useless noise or background. The independence of random variables, as a basic concept in statistics is hard to compute and distinguish, hence, how to approximately calculate independence is of great significance on the results of BSS. In addition, ICA, a classical unsupervised learning algorithm, gives the effective results on the signal processing. For example, based on the different physical technology of the modern medicine, the received brain imaging assists medics to conduct in-depth research on patients' conditions with mixing signals, such as electroencephalogram (EEG) [40], functional near-infrared spectroscopy (FNIRS) [43], functional magnetic resonance imaging (MRI) [11] and so on.

The sparse representation has already applied on image processing as a common technique of feature extraction, such as image super-resolution [29, 46]; and image restoration [42]. Moreover, the RFs produced by sparsity maximization is quite similar to those of simple cells when the inputs are natural image. In fact, the independent features from the natural image could generate a sparse representation since in some aspect the super-gaussianity is equivalent to sparseness [45]. The conventional ICA attempts to illuminate sparse coding analysis via approximating the independence of the variables.

However, the factorization of multiple variables cannot be directly applied on the conventional independent features learning algorithm owing to the ambiguity of the nongaussianity. Hence, in the conventional ICA, a major of works are about the approximate measure of the independence or non-gaussianity of different variables, such as the mutual information [40], kurtosis [10], negentropy [37] and mutual information rate [18].

Ordinarily the complicated relationship and diversity of data originate in the multiple factors of practical issue and clarify via signal processing in V1. For simple and complex cells in V1, there simultaneously exists the linear and nonlinear transformations in order to extract the features and imitate the demixing process in the real scenarios [35].

Therefore, partial independence implies that the dependent features exist inside the independent subspace through a linear transformation rather than the simplified mutual independence in conventional ICA. Laplace pdf are regarded as the super-gaussian (sparse) pdf in approximately seeking for the features by independent subspace analysis (ISA), where the independence cannot be quantified [34].

Some of the independent filters resemble Gabor filters as the perception of edge detectors in the human

visual system from the natural image data [35]. In addition, the characteristic of conventional ICA features are thought to be similar with the RFs of simple cells in V1 [18, 20, 34].

In this paper, we are motivated to relax the constraints of ICA by involving the difference of the independent subspace and realize the operation mechanism of the brain in V1 based on the natural images to modify the complex cells. The rest of the paper is organized as follows. Section 2 illustrates how to redeclare the connection between independence and non-gaussianity with the change of independence assumption and how to validate the properties of complex cells based on the characters of complex cells in V1. In Section 3, the maximum likelihood of supergaussian pdf optimize complete features AISA model updating the multiple parameters by CD algorithm. The experiments in Section 4 are applied on the pixel blocks clipped from natural image to learn the features and filters of AISA after dimensional reduction and whitened or sphering preprocessing. The energy correlation of the AISA results illustrates the differences on independence between inside subspace and outside subspace. Compared with the features of other ICA, the features of AISA are invariant to phase and shift and selectivity to frequency and orientation successfully verified by tuning curve test.

2. Background

More than eighty percent of the external information perceived by the human brain are derived from the visual channel and handled by millions of cells in brain with nervous impulse [25]. Initially, the independence involved is attempted to imitate the information processing that human beings can autonomously select the useful information, and simultaneously ignore the useless noise or background [3, 18, 40]. The distinct types of independence among the variables directly influence the complex relationship of sources and determine a specific approach to explore the connection between the independence and non-gaussianity. In addition, the primary visual cortex (V1) impacts on the perception of human beings with both simple cells and complex cells, where tuning curve test is used for verifying the properties of complex cells explored by electrochemical stimulation based on neuroscience [5,20].

2.1. Non-Gaussianity

The mutually independent sources in conventional ICA, should be either non-gaussian random variables, including only super-gaussian and sub-gaussian random variables, or no more than one gaussian random variable in terms of central limit theorem [5]. The scholars have conducted in-depth researches on the equivalency between the mutual independence and non-gaussianity [22, 40], and successfully applied the negentropy, a measure of non-gaussianity to approximate independence on BSS problem [18]. However, it is not confined to the practical issues with the strong assumption of the independence among the variables [4, 9].

The partial independence is based on the process of abstract practical problems, and the main purpose is to relax the completely independent constraint of ICA and maintain the dependence of subspace. However, the problem with the local independence hypothesis is how to maximize the unknown transformation in the subspace and the independence outside the subspace.

The general form of the super-gaussian distribution [34] is given by

$$p(x) = exp\left(-\alpha x^{r} + \beta\right), \tag{1}$$

where $\alpha > 0$ and $r \in (0, 2)$. According to the normalization of (1), β is expressed as

$$\exp(\beta) = \frac{r\alpha^{\frac{1}{r}}}{\Gamma(\frac{1}{r})}.$$

Excess kurtosis [47] as a measure of the tailedness of a real-valued random variable is a descriptor of the steep shape of a probability distribution relative to a standard normal distribution

$$K(x) = \frac{\sum_{i=1}^{N}(x_i - \overline{x})^4 / N}{s^4} - 3, \tag{2}$$

where x denotes the mean of x, s represents the standard deviation of x, and Nindicates the number of data points. For example, a positive excess kurtosis of any univariable distribution is a super-gaussian distribution. The steep shape of the pdf depends on the multi-parameters α and r respectively in (1), where the kurtosis of super-gaussian pdf stay the same when α is less than 3, and shown in Figure 1.

Figure 1

Kurtosis of super-gaussian pdf. The kurtosis in (2) is calculated by 10,000 data sampling from the super-gaussian pdf according to (1) with _ ∈ [1; 5] and r ∈[0:01; 1:99]

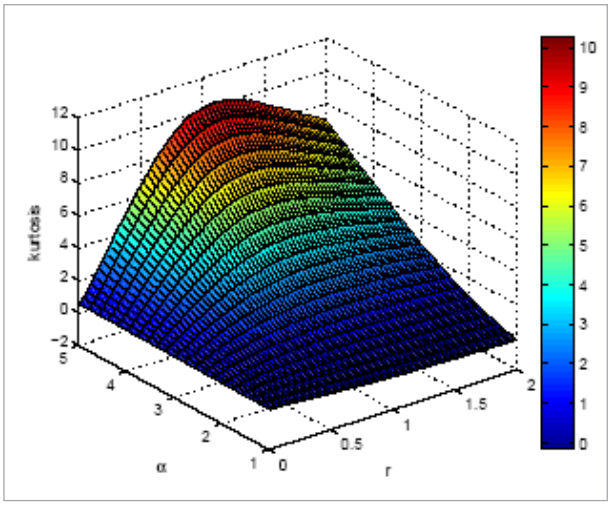

Moreover, sparseness is basically consistent with the super-gaussianity since its property are close to zero while the super-gaussian pdf has a peak at zero with a positive excess kurtosis [41]. As a consequence, the norm of recovery sources in the independent subspace obeys the super-gaussian pdf.

However, the projection of data in one subspace plays a modest role in influencing the sparseness [15, 31]. Therefore, for simplicity, the features in one subspace are related with each other based on linear transformation, somewhat analogous to the assumption of linear transformation in conventional ICA.

Since the diversity of data normally exists and obeys the super-gaussian distribution, the super-gaussianity is prevalent to study the process of the hidden information in the mixing signals in order to discriminate the different sources. Consequently, the diversity of partial independence have been introduced to obtain an adaptive independent subspaces analysis (AISA) algorithm involving the general form of the super-gaussian pdf in Section 3.

2.2. Primary Visual Cortex

Artificial intelligence (AI) increasingly prevails in processing the information by imitating the unique approaches of human beings [24]. Most neurons in V1 respond strongly to the oriented lines (edges or bars) moving into a preferred direction, and are selective to line orientation for a great extent by the receptive field structure (RFs) [8, 14]. An active area of advances aims at building a realistic models of RFs that could clarify neuronal responses to the different stimulus. Information processing initially originates with most of inputs from luminous stimulus into electrochemical signals repeatedly transformed by the algorithms of both bottom-up and top-down processing in brain.

The primary visual area (V1) of cerebral cortex is deemed to be the first stage of cortical processing of visual information. The RFs of neurons involved in V1 are a complicated combination of linear and nonlinear transformation and therefore hard to characterize in mathematics, especially in the context of natural stimulus [38]. The linear RFs of simple cells have spatial summation within both the excitatory and inhibitory regions [27]. Moreover, the nonlinear RFs of complex cells are invariant to phase and selective to the orientation or spatial frequency tuning of the neurons [39].

Tuning curves are extensively applied to portray the responses of neurons in V1 for the external (natural) stimulus when the stimulus at their peak, which evoke the highest firing rates, are the most significant to a neuron. Tuning curve test (analysis of selectivity) is applied to characterize complex cells based on the grating function, i.e. sinusoidal function [44]

$$\begin{cases} f_1(x,y) = \sin(2\pi\alpha(sin(\theta)x + cos(\theta)y)) \\ f_2(x,y) = \cos(2\pi\alpha(sin(\theta)x + cos(\theta)y)) \end{cases}, \quad (3)$$

where the frequency α, orientation or angle θ determine the oscillation and the x axis is corresponding to $\theta = 0$. The two functions f_1, f_2 obtain two oscillation in quadrature-phase (90 degrees phase) in precise. In order to accomplish tuning curve test, these grating functions are firstly computed and normalized to unite norm for a large number of orientations and frequencies. Then, the optimal frequency α_{opt} and orientation θ_{opt} are obtained by maximizing the sum of squares of the corresponding functions f_1, f_2 by using the two dot-product between the features in the subspace and each grating. Similarly, the selectivity of the phase is analyzed with the optimal frequency and orientation.

3. The Adaptive Learning Rule

In this section, the constraint of mutual independence in conventional ICA is relaxed by involving the mutual independent subspace and introducing the disparity of subspaces with the general form of super-gaussian pdf rather than the Laplace pdf in ISA [34].

Analogous to the linear transformation in ICA [5, 13, 37], the features are assumed to have linear relation with others in interior subspace.

Thereinto, the square of the norm of the linear projection of data z_j is given by

$$z_j = \sum_{i \in S_j} y_j^2 = \sum_{i \in S_j} <w_i, X>^2 \tag{4}$$

with the received mixing data X and j_{th} subspace composed by $w_i, i \in S_j$.

Then, the adaptive independent subspace analysis model is built on the super-gaussianity of z_j in basis of the sparseness of the norm of projection of visual data on any subspace [15]. The learning rule is conceived in terms of estimating multi- parameter that maximize the likelihood of z_j based on the general super-gaussian pdf.

Rather than the factorability of independent multi-variable

$$P(X) = P(x_1, x_2, \cdots, x_n) = \prod_{j=1}^{n} P(x_j) \tag{5}$$

mutual information, kurtosis and negentropy are originally applied to approximately calculate the independence of sources. Nevertheless, we apply super-gaussian distribution via the factorability of independent multi-variable on the norm of the projection of data in the independent subspace. Therefore, the complete AISA model is given by

$$\begin{aligned} &\max_{W,\Lambda,R} && E\{L(Z)\} = \sum_{j=1}^{n} E_X\{\log(p(z_j))\} \\ &s.t. && W^T W = I \end{aligned} \tag{6}$$

where $P(z_j) = exp(-\alpha_j \| z_j \|_2^{r_j} + \beta_j)$, $\Lambda = (\alpha_1, \alpha_2, \cdots, \alpha_n)$, $\alpha_j \in (0, +\infty)$, $R = (r_1, r_2, \cdot, r_n)$, $r_j \in (0,1)$ and the row of W is $w_i = (w_{1i}, w_{2i}, \cdots, w_{ni})$. According to the normalization of super-gauss distribution, the expectation likelihood function E of the partial independent component Z is given by:

$$\begin{aligned} E_X\{L(Z)\} &= E_X\{\log \prod_{j=1}^{n} \frac{1}{E(\theta_j)} \exp(-\alpha_j (z_j)^{r_j})\} \\ &= \sum_{j=1}^{n} (-\log E(\theta_j) - E_X\{\alpha_j (z_j)^{r_j}\}), \end{aligned} \tag{7}$$

where $\theta_j = (w_{i(i \in S_j)}, \alpha_j, r_j)$.

The independent subspace $S_j, j = 1, 2, \cdots, n$ in (4) are hard to count, similar to the number of the functional neurons in brain. The subspace size has the ambition composed by the uniform elements of square sub-matrix. According to a constant subspace size for the sake of simplicity, for instance, on the basis of 2–dimensional subspace, the matrix H conducts as the independent subspace in AISA and is depicted by the second order square matrix with uniform elements in the following block diagonal matrix.

Now therefore, the complete AISA model (6) is rewritten by

$$\begin{aligned} &\max_{W,\Lambda,R} && \sum_{j=1}^{n} (-\log E(\theta_j) - E_X(\alpha_j (\sum_{i=1}^{|S_j|} <w_i, X>^2)^{r_j})) \\ &s.t. && W^T W = I, \end{aligned} \tag{8}$$

where $\Lambda = (\alpha_1, \alpha_2, \cdots, \alpha_n)$ and R $R = (r_1, r_2, \cdots, r_n)$. Whitened or sphering preprocessing as a basic trick in ICA in terms of $E\{X\} = 0$ and $E\{XX^T\} = I$, where I is the identity matrix, and the normalization factor $E(\theta_j)$ is explained in Appendix A in details. The approximate expectation of $\frac{\partial \alpha_j z_j^{r_j}}{\partial \theta_j}$ could be achieved by MCMC resampling method with k steps under $P(z_j; \theta_j)$. In consequence, instead of the basic gradient of the multi-parameter Λ and R in (8), the approximation CD method facilitates to obtain the fast updating formulas given as following:

$$\begin{cases} \dfrac{\partial E_X\{L(Z)\}}{\partial \alpha_j} = < z_j^{r_j} >_{Z_{jk}} - < z_j^{r_j} >_{Z_{j0}} \\ \dfrac{\partial E_X\{L(Z)\}}{\partial r_j} = < \alpha_j z_j^{r_j} \log z_j >_{Z_{jk}} - < \alpha_j z_j^{r_j} \log z_j >_{Z_{j0}} \end{cases}, \tag{9}$$

where $< \cdot, \cdot >_{Z_{jk}}$ is the is the expectation with k steps resampling Z_{jk} under $P(z_j; \theta_j)$.

Then $w_i, i \in S_j$ should be optimized in sequence under the assumption of the subspace matrix H. Hence, after the updating multi-parameters α_j and r_j in the subspace S_j, $w_i, i \in S_j$, is updated by the gradient of (8) given by:

$$\frac{\partial E_X\{L(Z)\}}{\partial w_i} \propto E_X\{-(z_j)^{(r_j-1)} y_j X\}. \quad (10)$$

At last, W should be ensured after the each iterative update in accordance with the constraint in formula (8) since that the orthonormality of Woriginates from the whitened processing for the sake of the ambiguity of independent source in ICA.

4. The Experiment

In this section, AISA features based on the natural image patches are ultimately verified with the phase and shift-invariance as well as frequency and orientation-selectivity.

Then the studies of AISA results make comparisons on the histogram of energy correlations both inside subspace and outside subspace, respectively. Moreover the sparseness is an another aspect to this property compared with the (log–)pdf's approximation of ISA features via Laplace pdf.

4.1. Natural Image Data

Natural images statistics are motivated by exploring the structures and working mechanism of biological visual systems in mammalian cerebral cortex. Simultaneously, the key to design a theoretical framework is to import the properties of the visual system so as to probe into the statistical structure of natural image data on account of evolutionary adaptation processes.

Consequently, natural image data1, including 13 photos with different size (256 × 512 and 512 × 256), have not any man-made architectures concerning the wild scene for research into natural image statistics, shown in Fig. 2(a). In Fig. 2(b), a 32 × 32 pixel block clips at the top left corner of the photo in the purple rectangle box. Then, four pixels are shifted in row and column in order to crop the photos into pixels blocks by the green rectangle and blue rectangle box, respectively. At last, 50, 000 image patches are randomly sampled from the above pixel blocks to obtain AISA feature and AISA filters via AISA algorithm. Due to the expectation of samples in (8), the arrangement of 50,000 image paths has few influence on the AISA results.

AISA features learning via the natural image data are more effective for driving complex cells, though the RFs measured with natural images were similar to those measured with random stimulus [39]. Hence, the natural image data are applied to learn AISA features as well as AISA filters in the following experiments.

Figure 2

Natural image data used as the stimulus to characterize omplex cells

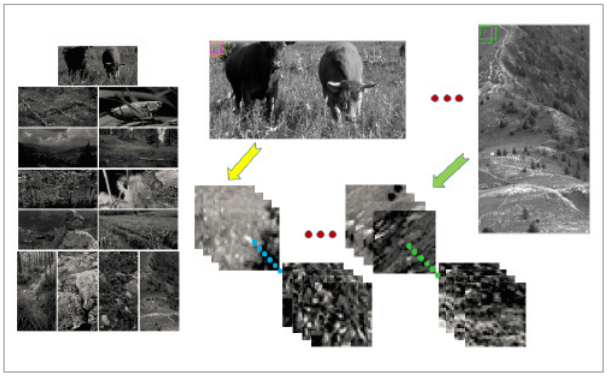

Left:13 photos are an accurate portrayal of natural surroundings without any man-made architectures, where these photos with different sizes (256 × 512 and 512 × 256) are applied on AISA learning rules to characterize complex cells and achieve the RFs of complex cells. Right: A 32 × 32 pixel block starts at the top left corner of the photo in the purple rectangle box. Then four pixels are shifted in row and column in order to crop the photos into 32 × 32 pixel blocks by the green rectangle and blue rectangle boxes, respectively. At last, 50; 000 image patches are randomly sampled from the above 32 × 32 pixel blocks in order to obtain AISA feature and AISA filters via AISA algorithm

4.2. The Partially Independent Features Learning from AISA

The principle component analysis (PCA) is commonly used for the dimension reduction in image processing in terms of removing the uncorrelation of variables. In accordance with the ambiguities of scale and direction in ICA, the whitened or sphering preprocessing also becomes a necessary and significant prerequisite for these image patches in AISA. The covariance matrix of these image patches X could be decomposed by singular value decomposition (SVD)

$$E\{XX^T\} = U\Sigma U^T, \quad (11)$$

where U is an orthogonal matrix and Σ is a positive diagonal matrix. Therefore, the combined preprocessing of the dimensionality reduction and whitened or sphering proceeds simultaneously by the project $X = \Sigma_m^{-2} U^T X$, where Σ_m is the first m row in matrix Σ. For simplicity, X is represented again after the combined preprocessing in the subsequent context.

In these experiments, the subspace dimensions S_j are set at 2, 4, 8, respectively, and the dimensionality

are reduced to 256. Moreover, X are used for updating the multiparameter $r_j, \alpha_j, w_i (i \in S_j)$ via (9) and (10) after the combined preprocessing with original learning rate $\mu = 0.1$, adjustable parameter of learning rate $\tau = 3/4$ and the maximum iteration $\gamma = 500$ in order to maximize AISA model (8).

The partially independent features, as well as filters are achieved by AISA based on 50, 000 image patches of 32 × 32 pixels blocks randomly sampling from natural image data. The filters of AISA in one subspace of 2–dimensional, 4–dimensional, 8–dimensional are one kind of Gabor filter located in the similar places as 'edge detectors' with the distinct frequencies, orientations and phases, especially 2-dimensional shown in Figure 3(a). The multi-group bases have a visual representation of the mixing matrix (AISA filters), where the bases in one group exists in the same subspace at the left of (a). The AISA filters in the same subspace demonstrate the 'edge detectors' in the dis-

Figure 3

The filters and features learning from AISA algorithm when trained on 50; 000 image patches under the assumption of 2–dimensional subspace. A visualizations of all groups of bases are produced by mixing matrix (AISA filters), where one group of bases exists in the same subspace at the left of (a). The AISA filters in the same subspace demonstrate the 'edge detectors' in the distinct frequencies, orientations and phases, similar to the Gabor filter, magnified at the right of (a). AISA features are shown at the left of (b), where six groups have the different edge information with varying the frequency, location and orientation, respectively, zooming in at the right of (b)

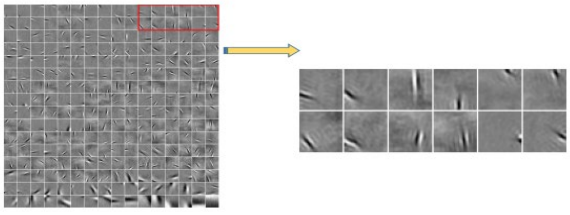

(a) AISA Filters

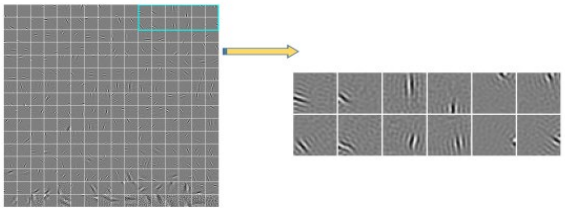

(b) AISA Features

Figure 4

The energy correlation analysis based on AISA features. According to the energy correlations of AISA results (a), the correlation of inside and outside subspace are generated by the column-value histogram in (b) and (c), respectively

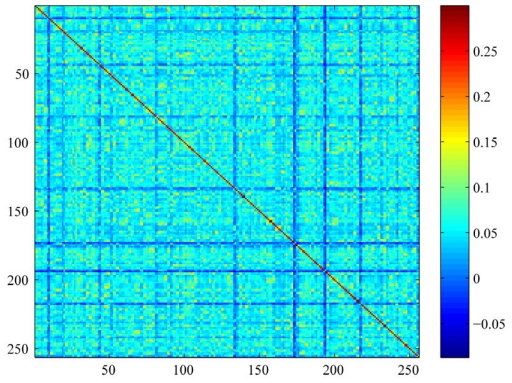

(a) The energy correlations of AISA results

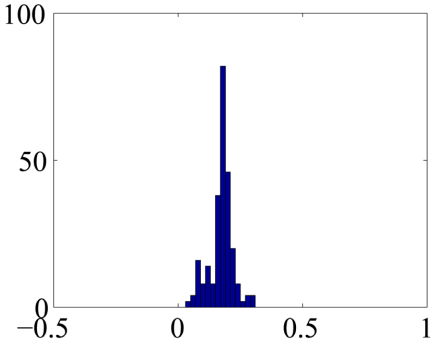

(b) Inside subspace correlations in AISA

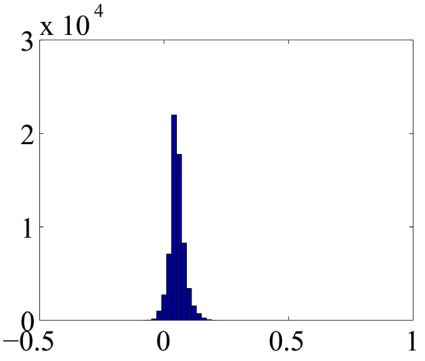

(c) Outside subspace correlations in AISA

tinct frequencies, orientations and phases, similar to the Gabor filter, magnified at the right of (a). Meanwhile, as can be seen in each group of bases in one subspace, AISA features acquire the boundary or edge information from the natural image patches, shown at the left of Figure 3 (b), where six groups have the different edge information with varying the frequencies, orientations and phases, zooming in at the right of (b).

According to the AISA results, the bases in one group have the similar shape of gratings with a small difference on the frequency, location and phase. Based on the AISA features, the energy correlations of AISA results or partial independent sources in one subspace are shown in Figure 4(a). The histogram is shown in Figure 4(c) that the energy correlations between the different subspace remain mostly close to zero, while the mid-value of energy correlations among the same subspace are approaching to 0.25, shown in Figure 4(b).

4.3. The Sparseness Measurement

According to the results of multiple parameters in AISA calculated by the CD algorithm, histogram of r_j and α_j are shown in Figure 5. Thereinto, values of r_j arrange unevenly from 0 to 1, while it is restricted to a specific value in ISA [34]). And the amounts of α_j decline with value increasing instead of ignoring it in ISA. The multiple parameters r_j and α_j have a significant influence on the sparsity in the super-gaussian pdf in Figure 1.

Figure 5

The value histogram of multiple parameters in AISA. After the AISA updating formulas, the multiple parameters are achieved, where the values of r_j arrange unevenly from 0 to 1 increasing, and the amounts of α_j decline with the value

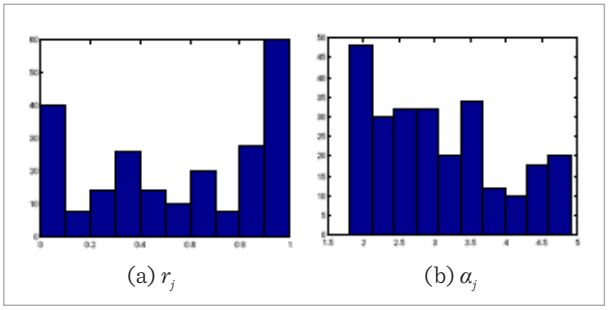

(a) r_j (b) α_j

A series of (log–) non-gaussian pdfs or sparse functions are fixed with $h(x) = log(cosh(x))$ in ICA [13, 37] and $p(x) = log(exp(-\sqrt{x}))$ in ISA. Instead, our proposed AISA algorithm are adaptive to update the sparse function via the multiple parameters r_j and α_j. The maximum likelihood estimation prompts the sparseness or super-gaussianity of partially independent sources in (8).

In principle, the maximum likelihood estimation is calculated with the original random initialization of r_j and α_j by updating $w_i, i \in S_j$. And then the likelihood function is recomputed by updating r_j and α_j with the optimal $w_i, i \in S_j$, where r_j and α_j determine the steep degree of super-gaussian pdf. The (log–) pdf's

Figure 6

Estimation of the optimal (log–) pdf's nonlinear function in the first 3 subspaces. Top row: feature. Bottom row: log–pdf's function

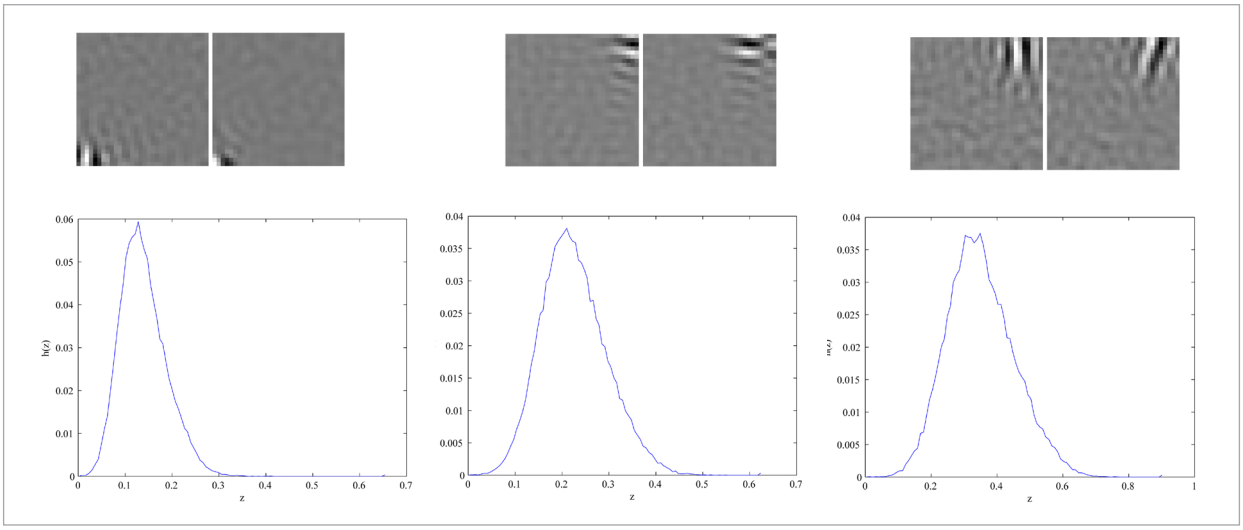

$h_j(\alpha_j, z_j, \beta_j)$ is given by:

$$h_j(\alpha_j, z_j, \beta_j) = \log p(z_j) = -\alpha_j z_j^{r_j} + \beta_j \quad (12)$$

According to AISA updating formula (9) and (10), $h_j(\alpha_j, z_j, \beta_j)$ could be a sparseness measure.

From the first 3 subspaces in Figure 3(b), the estimation of the optimal (log-) pdf's nonlinear function $h_j, j = 1,2,3$ are shown in Figure 6.

4.4. The Emergence of Phase and Shift-Invariant Feature

The phase and shift-invariant features embody the hallmark properties of complex cells in V1 that responds for the bar or edge of some particular orientation and location. Namely, the response of complex cells is unaltered with the bars or simulations of a series of changes in direction.

Tuning curve test (analysis of selectivity) is routinely executed by using drifting gratings with the maximum response of complex cells in V1. The optimal phase, frequency and orientation are calculated by the traversing method. The achieved respondence curves of the first ten AISA features separately vary one of the three optimal degrees of freedom: phase (translation), frequency and orientation (rotation), shown in Figure 7. The two AISA features respond to the energy detectors of tuning curve with phase-invariance, frequency- and orientation-selectivity.

Figure 7

The response of the first 10 features learning from AISA algorithm varying its three degrees of freedom: phase, frequency and orientation, respectively. The *x*-axes are variations in phase/frequency/orientation. The y-axes are the normalized activations of cells. According to tuning curve of the response energy detectors, features of AISA algorithm are selective to frequency and orientation, invariant to phase

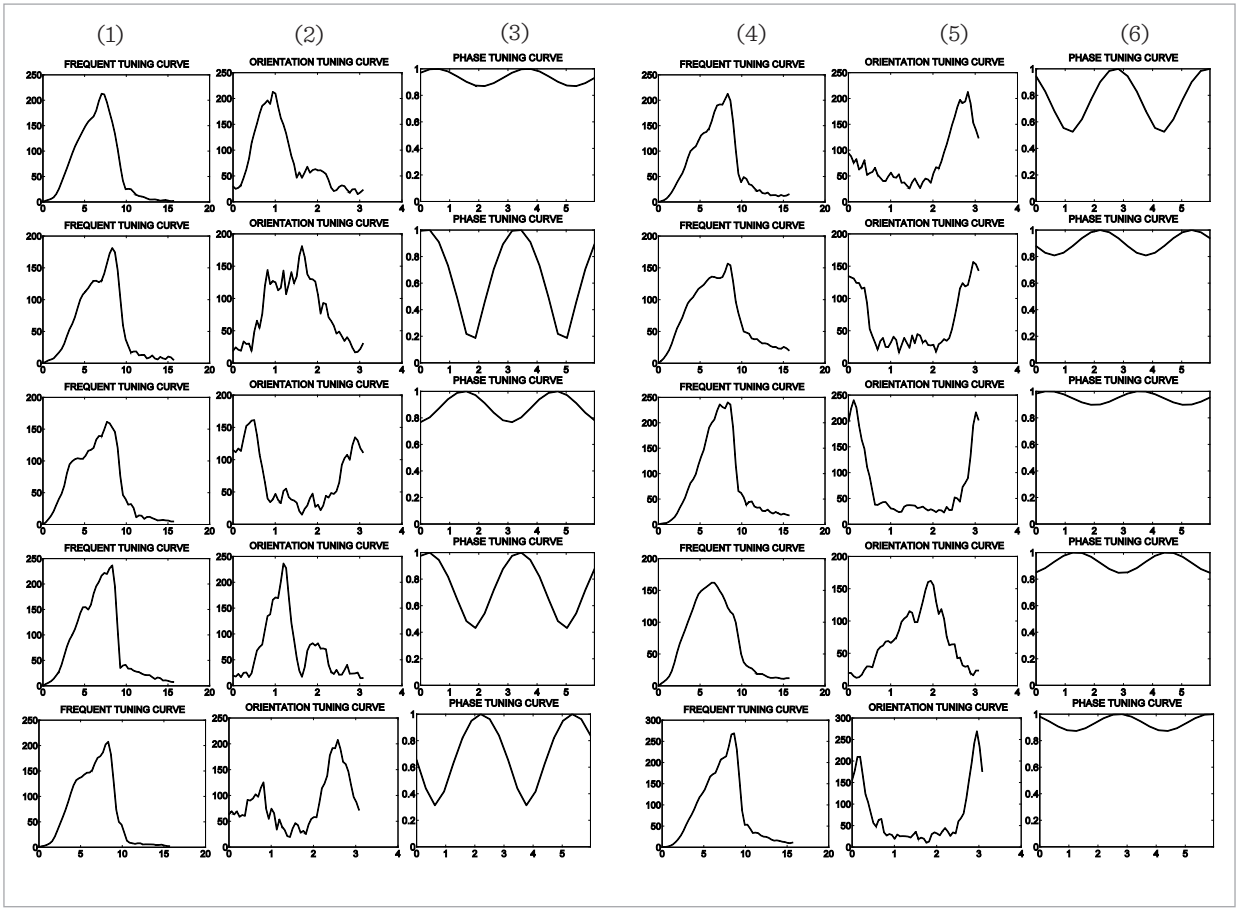

In reality, it is difficult to distinguish between phase-invariance and position invariance, also known as shift-invariance. In other words, the features learning via AISA algorithm are robust to local translation (phase) while being selective to frequency and orientation (rotation). This combination of robustness and selectivity makes features learned by AISA algorithm highly invariant [6, 21, 44]. This shows that AISA demonstrates emergence of properties similar to those of complex cells.

5. Conclusion

We proposed an adaptive independent subspace analysis to learn phase and shift-invariant features which characterize complex cells in V1. Rather than the conventional 'independent component', the partial independent component are depicted by the general form of super-gaussian distribution function. CD algorithm is used to solve AISA model and update the sparseness measure function h_j.

The properties of independence by higher order statistic are much stronger than the properties of un-correlatedness that form principle component analysis (PCA) based on the second order statistic [45]. The filters and features learning from PCA generates the spatially global properties (the whole) instead of the local properties (details, parts) based on ICA. In the brain and cognitive sciences, the cells firstly extract the essential local features accompanied with ignoring the shift and rotation transformation. Then a global structure is constructed with the combination of the local feature so as to improve the effectiveness in coping with practice issues.

ICA makes a strong constraint on the mutual independence to simplify the practice issues. And the features characterize the properties of simple cell with the assumption of linear transformation in the mixing and demixing proceeding. Nevertheless, the properties of partial independence make a more approximation on the complex information processing in the brain cells.

Independent subspace analysis (ISA) focus on a common case where partial independent is considered rather than independent completely and regardless of the difference in the subspace. The updating rule are derived from the special super-gaussian distribution, Laplace distribution, with an approximate solution. The combination of independence and invariant subspace in ISA overcomes the constraints of the nonlinear transformation.

Our proposed AISA is more pervasive rather than ICA and ISA. Firstly, the phase and shift-invariance of AISA features are verified via the tuning curve test. AISA focus on a common situation with partial independent less than independent completely with the subspace difference. Furthermore, ISA is a special case of AISA, when the parameters of standard super-gaussian pdf in AISA is fixed. Later we attempt to apply the AISA algorithm into classification task based on the local information in details.

At last, we will relax the constraint of subspace size and extend the model with label information in the future works.

Acknowledgment

This job is supported by the National key R&D Program of China under Grant NO. 2018YFB0203901. This work is also supported by the Key Research and Development Program of Shaanxi Province(-No.2018ZDXM-GY-036) and the National Natural Science Foundation of China (No.61572393, 61877049, 11671317).

Appendix

The norm of the projection of visual data on practically any subspace has a supergaussian distribution. Meanwhile, pdf of independence of multi-variable is equal to the factorization of the variables.

$$E_X\{L(Z)\} = \log E_X\{P(Z)\} = \log(\prod_{j=1}^{n} P(z_j)) = -\sum_{j=1}^{n}(\log E(\theta_j) + \alpha_j z_j^{r_j}),$$

where $r_j \in (0,1)$, $\theta_j = (\alpha_j, r_j)$ and $\theta = (\theta_1, \theta_2, \cdots, \theta_n)$. Then the complete AISA model is built in the following:

$$\max_{W,\Lambda,R} \quad E_X\{L(Z)\} = E_X\{\sum_{j=1}^{n} \log(p(z_j))\}$$
$$s.t. \quad W^T W = I,$$

where $P(z_j)=\frac{1}{E(\theta_j)}exp(-\alpha_i z_j^{r_j})$, $\Lambda=(\alpha_1,\alpha_2,\cdots,\alpha_n)$, $R=(r_1,r_2,\cdot,r_n)$, $r_i\in(0,1)$ and the row of W is $w_i=(w_{1i},w_{2i},\cdots,w_{ni})^T$.

$$\begin{aligned}
&\frac{\partial E_X\{-L(Z)\}}{\partial\theta_j}\\
=&\frac{1}{E(\theta_j)}\frac{\partial E(\theta_j)}{\partial\theta_j}+\frac{\partial E_X\{\alpha_j z_j^{r_j}\}}{\partial\theta_j}\\
=&\frac{1}{\int\exp(-\alpha_j z_j^{r_j})dz_j}\int\frac{\partial\exp(-\alpha_j z_j^{r_j})}{\partial\theta_j}dz_j+E_X\{\frac{\partial\alpha_j z_j^{r_j}}{\partial\theta_j}\}\\
=&\int\frac{\exp(-\alpha_j z_j^{r_j})}{\int\exp(-\alpha_j z_j^{r_j})dz_j}\frac{\partial(-\alpha_j z_j^{r_j})}{\partial\theta_j}dz_j+E_X\{\frac{\partial\alpha_j z_j^{r_j}}{\partial\theta_j}\}\\
=&<\frac{\partial\alpha_j z_j^{r_j}}{\partial\theta_j}>_{z_{j0}}-<\frac{\partial\alpha_j z_j^{r_j}}{\partial\theta_j}>_{P(z_j;\theta_j)}
\end{aligned}$$

The gradient for α_j and r_j is given by:

$$\begin{aligned}
\frac{\partial E_X\{L(Z)\}}{\partial\alpha_j}&=<z_j^{r_j}>_{Z_{jk}}-<z_j^{r_j}>_{Z_{j0}}\\
\frac{\partial E_X\{L(Z)\}}{\partial r_j}&=<\alpha_j z_j^{r_j}\log z_j>_{Z_{jk}}-<\alpha_j z_j^{r_j}\log z_j>_{Z_{j0}}
\end{aligned}$$

Then how to resample from the $P(Z)$ is essential for AISA algorithm. According to $E\{XX^T\}=I$, the mean of z_j can be obtained

$$E\{z_j\}=\sum_{i\in S_j}w_i^T E\{XX^T\}w_i=\|S_j\|$$

where $\|S_j$ is the cardinal number of the set S_j. In order to simply the problem, we could define the j_{th} subspace S_j in advance by matrix H.

$$\begin{aligned}
&\int z_j P(z_j;\theta)dz_j=\int z_j\frac{\exp(-\alpha_j z_j^{r_j})}{E(\theta_j)}dz_j=\|S_j\|\\
&E(\theta_j)=\frac{\int z_j\exp(-\alpha_j z_j^{r_j})dz_j}{\|S_j\|}
\end{aligned}\tag{13}$$

As for the discrete variable, the integration could be rewritten as

$$E(\theta_j)=\frac{\sum_{z_j}z_j\exp(-\alpha_j z_j^{r_j})}{\|S_j\|}\tag{14}$$

References

1. Andermann, M. L., Kerlin, A. M., Roumis, D. K., Glickfeld, L. L., Reid, R. C. Functional Specialization of Mouse Higher Visual Cortical Areas. Neuron, 2011, 72(6), 1025-1039. https://doi.org/10.1016/j.neuron.2011.11.013
2. Basiri, S., Ollila, E., Koivunen, V. Alternative Derivation of FastICA with Novel Power Iteration Algorithm. IEEE Signal Processing Letters, 2017, (99), 1-1. https://doi.org/10.1109/LSP.2017.2732342
3. Bell, A. J., Sejnowski, T. J. An Information-Maximization Approach to Blindseparation and Blind Deconvolution. Neural Computation, 1995, 7(6), 1129-1159. https://doi.org/10.1162/neco.1995.7.6.1129
4. Benveniste, A., Goursat, M., Ruget, G. Robust Identification of a Nonminimum Phase System: Blind Adjustment of a Linear Equalizer in Data Communications. IEEE Transactions on Automatic Control, 1980, 25(3), 385-399. https://doi.org/10.1109/TAC.1980.1102343
5. Cardoso, J. F. Dependence, Correlation and Gaussianity in Independent Component Analysis. Journal of Machine Learning Research, 2003, 4(Dec), 1177-1203.
6. Chen, P., Qi, Y., Li, X., Hou, D., Lyu, M. R.-T. ARF-Predictor: Effective Prediction of Aging-Related Failure Using Entropy. IEEE Transactions on Dependable and Secure Computing, 2016, 1-1. https://doi.org/10.1109/TDSC.2016.2604381
7. Chen, X., Han, F., Poo, M. M., Dan, Y. Excitatory and Suppressive Receptivefield Subunits in Awake Monkey Primary Visual Cortex (V1). Proceedings of the Natio-

nal Academy of Sciences, 2007, 104(48), 19120-19125. https://doi.org/10.1073/pnas.0706938104

8. Cheong, S. K., Tailby, C., Solomon, S. G., Martin, P. R. Cortical-Like Receptive Fields in the Lateral Geniculate Nucleus of Marmoset Monkeys. The Journal of Neuroscience, 2013, 33(16), 6864-6876. https://doi.org/10.1523/JNEUROSCI.5208-12.2013
9. Cram'er, H. Mathematical Methods of Statistics (PMS-9) (Vol. 9). Princeton university press, 2016.
10. Fu, G. S., Phlypo, R., Anderson, M., Li, X. L., Adali, T. Blind Source Separation by Entropy Rate Minimization. IEEE Transactions on Signal Processing, 2014, 62(16), 4245-4255. https://doi.org/10.1109/TSP.2014.2333563
11. Funane, T., Atsumori, H., Katura, T., Obata, A. N., Sato, H., Tanikawa, Y., Kiguchi, M. Quantitative Evaluation of Deep and Shallow Tissue Layers' Optodes and Independent Component Analysis. Neuroimage, 2014, 85, 150-165. https://doi.org/10.1016/j.neuroimage.2013.02.026
12. Ganguli, S., Sompolinsky, H. Compressed Sensing, Sparsity, and Dimensionality in Neuronal Information Processing and Data Analysis. Annual Review of Neuroscience, 2012, 35, 485-508. https://doi.org/10.1146/annurev-neuro-062111-150410
13. Goodfellow, I. J., Le, Q. V., Saxe, A. M., Lee, H., Ng, A. Y. Measuring Invariances in Deep Networks. International Conference on Neural Information Processing Systems. Curran Associates Inc., 2009.
14. Henriksen, S., Tanabe, S., Cumming, B. Disparity Processing in Primary Visual Cortex. Philosophical Transactions of the Royal Society B, 2016, 371(1697), 20150255.
15. 15. Horwitz, G. D., Chichilnisky, E. J., Albright, T. D. Cone Inputs to Simple and Complex Cells in V1 of Awake Macaque. Journal of Neurophysiology, 2007, 97(4), 3070-3081. https://doi.org/10.1152/jn.00965.2006
16. Hosoya, H., Hyvärinen A. Learning Visual Spatial Pooling by Strong PCA Dimension Reduction. Neural Computation, 2016, 28(7), 1249-1264. https://doi.org/10.1162/NECO_a_00843
17. Hyvärinen, A., Oja, E. Independent Component Analysis: Algorithms and Applications. Neural Networks, 2000, 13(4), 411-430. https://doi.org/10.1016/S0893-6080(00)00026-5
18. Hyvärinen, A., Hoyer, P. Emergence of Phase-and Shift-Invariant Features by Decomposition of Natural Images Into Independent Feature Subspaces. Neural Computation, 2000, 12(7), 1705-1720. https://doi.org/10.1162/089976600300015312
19. Hyvärinen, A., Hurri, J., Hoyer P. O. Natural Image Statistics: A Probabilistic Approach to Early Computational Vision. Computational Imaging and Vision, Springer Publishing Company, Incorporated, 2009. https://doi.org/10.1007/978-1-84882-491-1
20. Hyvärinen, A. Independent Component Analysis: Recent Advances. Philosophical Transactions of the Royal Society A, 2013, 371(1984), 20110534.
21. Isomura, T., Toyoizumi, T. Error-Gated Hebbian Rule: A Local Learning Rule for Principal and Independent Component Analysis. Scientific Reports, 2018, 8(1835).
22. Joseph, A., Navin, G., Anupama, N., Luis, R. Heavy-Tailed Analogues of the Covariance Matrix for ICA. AAAI, 2017, 1712-1718.
23. Karklin, Y., Lewicki, M. S. Emergence of Complex Cell Properties by Learning to Generalize in Natural Scenes. Nature, 2009, 457(7225), 83-86. https://doi.org/10.1038/nature07481
24. Kay, K. N., Naselaris, T., Prenger, R. J., Gallant, J. L. Identifying Natural Images from Human Brain Activity. Nature, 2008, 452(7185), 352-355. https://doi.org/10.1038/nature06713
25. Lindsay, P. H., Norman, D. A. Human Information Processing: An Introduction to Psychology. Science, 1971, 174(4010), 683-684.
26. Milan, S., Roger, B., Vaclav, H. Image Processing, Analysis, and Machine Vision. Chapman & Hall Computing, 1993.
27. Nauhaus, I., Nielsen, K. J., Callaway, E. M. Efficient Receptive Field Tiling in Primate V1. Neuron, 2016, 91(4), 893-904. https://doi.org/10.1016/j.neuron.2016.07.015
28. Olshausen, B. A., Field, D. J. Emergence of Simple-Cell Receptive Field Properties by Learning a Sparse Code for Natural Images. Nature, 1996, 381(6583), 607-609. https://doi.org/10.1038/381607a0
29. Peleg, T., Elad, M. A Statistical Prediction Model Based on Sparse Representations for Single Image Super-Resolution. IEEE Transactions on Image Processing, 2014, 23(6), 2569-2582. https://doi.org/10.1109/TIP.2014.2305844
30. Pham, D. T. Blind Separation of Instantaneous Mixture of Sources Via an Independent Component Analysis. IEEE Transactions on Signal Processing, 1996, 44(11), 2768-2779. https://doi.org/10.1109/78.542183
31. Posner, M. I., Petersen, S. E. The Attention System of the Human Brain. Annual Review of Neuroscience, 1990, 13(1), 25-42. https://doi.org/10.1146/annurev.ne.13.030190.000325

32. Qiao, K., Zhang, J., Song, H., Wan, Y. Big Data Analytics Enabled by Feature Extraction Based on Partial Independence. Neurocomputing, 2017, 288, 3-10. https://doi.org/10.1016/j.neucom.2017.07.072
33. Roth, M. M., Helmchen, F., Kampa, B. M. Distinct Functional Properties of Primary and Posteromedial Visual Area of Mouse Neocortex. The Journal of Neuroscience, 2012, 32(28), 9716-9726. https://doi.org/10.1523/JNEUROSCI.0110-12.2012
34. Russ, J. C. The Image Processing Handbook. CRC Press, 2002.
35. Saremi, S., Sejnowski, T. J., Sharpee, T. O. Double-Gabor Filters are Independent Components of Small Translation-Invariant Image Patches. Neural Computation, 2013, 25(4), 922-939. https://doi.org/10.1162/NECO_a_00418
36. Sedigh-Sarvestani, M., Fernandez-Lamo, I., Jaegle, A., Taylor, M. M. Second Order Receptive Field Properties of Simple and Complex Cells Support a New Standard Model of Thalamocortical Circuitry in V1. The Journal of Neuroscience, 2014, 34(34), 11177-11179. https://doi.org/10.1523/JNEUROSCI.2425-14.2014
37. Tan, A. Y., Chen, Y., Scholl, B., Seidemann, E., Priebe, N. J. Sensory Stimulation Shifts Visual Cortex from Synchronous to Asynchronous States. Nature, 2014, 509(7499), 226-229. https://doi.org/10.1038/nature13159
38. Tichavsky, P., Koldovsky, Z., Oja, E. Performance Analysis of the FastICA Algorithm and Crame/spl Acute/r-rao Bounds for Linear Independent Component Analysis. IEEE Transactions on Signal Processing, 2006, 54(4), 1189-1203. https://doi.org/10.1109/TSP.2006.870561
39. Touryan, J., Felsen, G., Dan, Y. Spatial Structure of Complex Cell Receptivefields Measured with Natural Images. Neuron, 2005, 45(5), 781-791. https://doi.org/10.1016/j.neuron.2005.01.029
40. Van Belle, J., Vink, M., Durston, S., Zandbelt, B. B. Common and Unique Neural Networks for Proactive and Reactive Response Inhibition Revealed by Independent Component Analysis of Functional MRI data. Neuroimage, 2014, 103, 65-74. https://doi.org/10.1016/j.neuroimage.2014.09.014
41. Wenger, E. Artificial Intelligence and Tutoring Systems: Computational and Cognitive Approaches to the Communication of Knowledge. Morgan Kaufmann, 2014.
42. Wright, J., Ma, Y., Mairal, J., Sapiro, G., Huang, T. S., Yan, S. Sparse Representation for Computer Vision and Pattern Recognition. Proceedings of the IEEE, 2010, 98(6), 1031-1044. https://doi.org/10.1109/JPROC.2010.2044470
43. Yang, J., Wright, J., Huang, T. S., Ma, Y. Image Super-Resolution via Sparse Representation. IEEE Transactions on Image Processing, 2010, 19(11), 2861-2873. https://doi.org/10.1109/TIP.2010.2050625
44. Yang, L., Han, J., Qi, Y., Wang, C., Gu, T., Liu, Y. Season: Shelving Interference and Joint Identification in Large-Scale RFID Systems. IEEE Transactions on Parallel & Distributed Systems, 2015, 26(11), 3149-3159. https://doi.org/10.1109/TPDS.2013.276
45. Zarzoso, V., Comon, P. Robust Independent Component Analysis by Iterative Maximization of the Kurtosis Contrast with Algebraic Optimal Step Size. IEEE Transactions on Neural Networks, 2010, 21(2), 248-261. https://doi.org/10.1109/TNN.2009.2035920
46. Zhang, J., Zhao, D., Gao, W. Group-Based Sparse Representation for Image Restoration. IEEE Transactions on Image Processing, 2014, 23(8), 3336-3351. https://doi.org/10.1109/TIP.2014.2323127
47. Zibulevsky, M., Pearlmutter, B. A. Blind Source Separation by Sparse Decomposition in a Signal Dictionary. Neural Computation, 2001, 13(4), 863-882. https://doi.org/10.1162/089976601300014385